Electrocatalysts

DOI: 10.1002/anie.201307527

Hydrogen Evolution by Tungsten Carbonitride Nanoelectrocatalysts Synthesized by the Formation of a Tungsten Acid/Polymer Hybrid In Situ**

Yong Zhao, Kazuhide Kamiya, Kazuhito Hashimoto, and Shuji Nakanishi**

The catalytic activity of early transition metal carbides, including their catalytic and mechanistic properties in various catalytic reactions,[1] has been actively studied since tungsten carbides were first found to display platinum-like behavior.[2] Previous reports have demonstrated that materials based on cost-effective tungsten carbide (WC) efficiently catalyze various reactions that require precious metal catalysts, including methane reformation, desulfurization, the hydrogen evolution reaction (HER), and ammonia decomposition.[3] Although progress has been made in improving catalytic performance, WC-based materials still have markedly lower catalytic activity and stability than noble metal catalysts in most experimental systems.

One of the strategies to improve the catalytic activity of metal-carbide-based materials is the introduction of other elements, which may appropriately tune the electronic state of the metal active site in a desirable direction. This strategy was shown to be effective for molybdenum carbide (MoC).[1a,4] When MoC and molybdenum nitride (MoN) were comparatively evaluated as catalysts for ammonia decomposition,[1a] MoN was found to be more active than MoC, a result that was possibly due to the abundance of highly energetic sites on the MoN catalyst for the rate-limiting N–N recombination step.

Nitridation of transition metals (or metal carbides) has been commonly done by direct ammonification at high temperatures.[1a] However, the as-generated metal (carbo)nitride materials suffer from crystal growth, incomplete ammonification, and low surface area,[5] resulting in a poorly crystalline structure and a low density of active sites. Due to these limitations in the material synthesis, metal (carbo)nitrides exhibited only moderate catalytic activities. Thus, a novel synthesis method for metal (carbo)nitrides is still needed.

In the present work, we developed a facile approach for the preparation of well-controlled tungsten carbonitride nanoparticles that overcomes the above limitations inherent in conventional synthesis methods (Figure 1). The resultant materials possess the following desirable characteristics: 1) uniformly small nanoparticles, 2) nitrogen-rich backbones, and 3) a pure tungsten carbonitride crystal structure. For the synthesis, polydiaminopyridine (PDAP) was first synthesized from the nitrogen-rich monomer diaminopyridine in the presence of Na_2WO_4. Protons released during the PDAP polymerization process reacted with soluble Na_2WO_4, resulting in the formation of hybrid nanomaterials in situ, which were composed of PDAP and insoluble H_2WO_4 nanoparticles (Supporting Information, Scheme S1). As iron is known to serve as a graphitization catalyst during pyrolysis, we pyrolyzed the hybrid materials in the presence of iron to form a N-rich tungsten carbonitride material (Fe-WCN; Figure 1a). We also prepared the materials pyrolyzed in the absence of Fe for a reference (WCN). Thus, this unique synthesis approach not only allows nanohybrids of H_2WO_4/PDAP polymer to be fabricated in a single step, but also supports the coordination of W species, owing to the high density of N sources from PDAP. The Fe-WCN materials

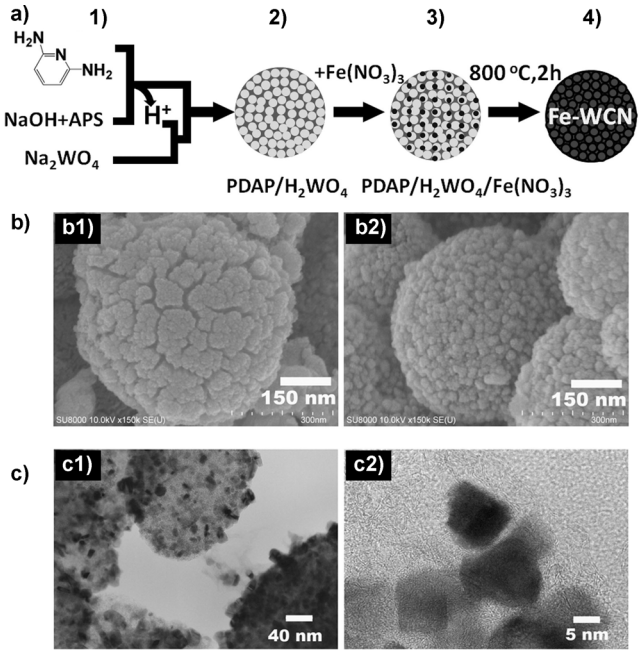

Figure 1. a) Synthesis of Fe-WCN materials. 1) PDAP + NaOH + APS + Na_2WO_4, 2) PDAP + H_2WO_4, 3) PDAP + H_2WO_4 + $Fe(NO_3)_3$, 4) Fe-WCN; gray dot H_2WO_4, black dot $Fe(NO_3)_3$, APS = ammonium persulfate. b) SEM images of WCN (b1) and Fe-WCN (b2) materials. c) TEM images of Fe-WCN materials synthesized at 800 °C.

[*] Dr. Y. Zhao, Dr. K. Kamiya, Prof. Dr. K. Hashimoto, Prof. Dr. S. Nakanishi
Department of Applied Chemistry, The University of Tokyo
7-3-1 Hongo, Bunkyo-ku, Tokyo 113-8656 (Japan)
E-mail: hashimoto@light.t.u-tokyo.ac.jp
nakanishi@light.t.u-tokyo.ac.jp

[**] We gratefully acknowledge the assistance of Shoichi Mastuda for the TEM and SEM measurements, and Dr. Youzhuan Zhang for the XRD analysis.

Supporting information for this article, including experimental details, is available on the WWW under http://dx.doi.org/10.1002/anie.201307527.

were characterized as model electrocatalysts for HER, and displayed efficient HER activities in both acidic and alkaline media, with an HER overpotential of about 100 mV and a tafel slope of about 47 mV dec^{-1} in acidic medium (pH 1), which is much better than that of tungsten carbonitride materials synthesized by traditional nitridation methods.

The morphologies of the pyrolyzed carbonitride (CN), WCN, Fe-WCN, and non-pyrolyzed PDAP/H_2WO_4 samples are shown in Figures 1b and S1. The CN material had a smooth spherical structure with a diameter of 500 nm (Figure S1a). After coordinating CN with W species, rough spheres covered with nanoparticles were formed (Figure 1b1). For Fe-WCN, numerous nanoparticles of ca. 10–20 nm in diameter were uniformly coated on the sphere surface (Figure 1b2). Large-scale images of the Fe-WCN samples showed that the porous spheres covered with nanoparticles were uniformly distributed (Figure S1c). Energy-dispersive spectroscopic SEM of the Fe-WCN samples confirmed that elemental W and Fe were well dispersed on the catalyst surface through X-ray mapping (Figure S2). SEM images of non-pyrolyzed H_2WO_4/PDAP revealed that the PDAP polymer spheres were uniformly covered by H_2WO_4 particles (Figure S1b, S1d). This finding confirmed our prediction that the synthetic process would efficiently deposit H_2WO_4 nanoparticles on/in the PDAP spheres.

The surface structure of the synthesized Fe-WCN materials was also examined by TEM. Figure 1c show the typical structures of the pyrolyzed Fe-WCN samples at 800 °C. The polymer spheres were uniformly coated by metallic nanoparticles of 10–20 nm in diameter, and no discernible difference in the size of the metallic particles was observed in Fe-WCN samples pyrolyzed at 800 °C or 900 °C (Figure S1e). This finding demonstrates that the pyrolysis temperature has only a minimal effect on the size of the metallic particles formed, possibly because the metallic particles were well dispersed on the carbon spheres. This property markedly differs from those of materials synthesized using previously reported methods.[5b] In addition, the crystal sizes of metallic carbide/nitride were markedly increased because of the fusion of metallic species at high temperatures.[5a,6]

The HER activity of the Fe-WCN materials was tested in H_2SO_4 solution (pH 1) using a rotating ring disk electrode (RRDE) system. To quickly remove and measure the evolved H_2 gas from the working and Pt ring electrodes, respectively, the rotation speed was set at 1000 rpm. Optimized Fe-WCN catalysts (Fe-WCN pyrolyzed at 800 °C for 2 h) were used, unless otherwise specified. We also measured and compared the HER activity of other reference materials, including bare glassy carbon, CN, FeCN, WCN, and commercial Pt/C catalysts (20 wt%). As shown in Figure 2a, the activities of glassy carbon, CN, and CN pyrolyzed with Fe (FeCN) materials for the HER were quite low. However, after introduction of W species into CN (WCN), the HER activity was substantially improved, based on the observed overpotentials and current density. Fe-WCN showed an even greater increase in HER activity compared to WCN. This difference was most likely due to the decreased electrical resistance of the Fe-WCN materials (0.5 Ω cm) compared with WCN (2.6 Ω cm). Additionally, the increased BET surface area of the Fe-WCN materials (127.2 $m^2 g^{-1}$) may result in a higher current density than that of WCN (79.2 $m^2 g^{-1}$).

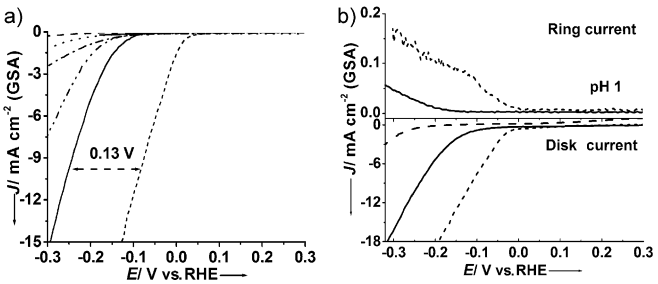

Figure 2. a) HER polarization curves of glassy carbon (– – –), CN-800 (••••), FeCN (–•–•), WCN-800 (–••–), Fe-WCN-800 (——), and commercial Pt/C (-----) catalyst in a pH 1 medium. b) H_2 gas evolved on the disk electrodes of a RRDE system; Fe-WCN (——), Pt/C (20 wt%; -----), c-Fe-WCN (– – –). Scan rate = 5 mV s^{-1}, rotational speed = 1000 r.p.m., catalyst loading = 0.4 mg cm^{-2}. c-Fe-WCN = conventional Fe-WCN, GSA = geometric surface area (0.2 cm^2).

Similar to the HER activity of Pt/C (0 V for overpotential, −10 mA cm^{-2} at −0.09 V_{RHE}), the Fe-WCN electrodes showed a 0.1 V HER overpotential and a current density of −10 mA cm^{-2} at −0.22 V_{RHE}. The potential gap at −10 mA cm^{-2} between the Fe-WCN and Pt/C materials was only 0.13 V, which is comparable to the most cost-effective electrocatalysts reported to date.[4,5c] Amperometric responses of the Pt ring electrode at a constant potential of 0.32 V_{RHE} were also monitored for detecting H_2 gas formed at the working electrode. As shown in Figure 2b, the evolved H_2 gas was detected on the Pt ring electrode for both Fe-WCN and Pt/C, suggesting that the Fe-WCN catalyst generated H_2 within the defined potentials. The HER stabilities of the synthesized Fe-WCN catalysts were evaluated using a sweeping potential in the RRDE system in H_2SO_4 solution. To prevent the possible influence of dissolved Pt species originating from the Pt counter electrode on HER activity, titanium wires were used as counter electrodes.[7] As shown in Figure S3, the catalytic current of the Fe-WCN electrode at the 3000th potential sweep was similar to that in the first sweep, thus demonstrating that the Fe-WCN catalyst generated a stable output of HER current.

We next attempted to detect the HER activities of Fe-WCN materials in alkaline medium (pH 13) using the RRDE system (Figure S4). Compared to the Pt/C catalyst (0 V for overpotential, −10 mA cm^{-2} at −0.1 V), the Fe-WCN materials exhibited an overpotential of 0.12 V and current density of −10 mA cm^{-2} at −0.25 V. These findings indicate that the Fe-WCN materials are also active in alkaline solution. We confirmed that the Fe-WCN catalysts had long-term stability in alkaline medium (Figure S4). Together, these results demonstrate that Fe-WCN catalysts can be used for H_2 generation over a wide pH range.

XPS was used to determine the surface elemental states of the CN, WCN, and Fe-WCN catalysts (Figure 3a and Table S1). The N 1s XPS spectra of the Fe-WCN materials were deconvoluted into three peaks (397.8 eV, 398.8 eV, and

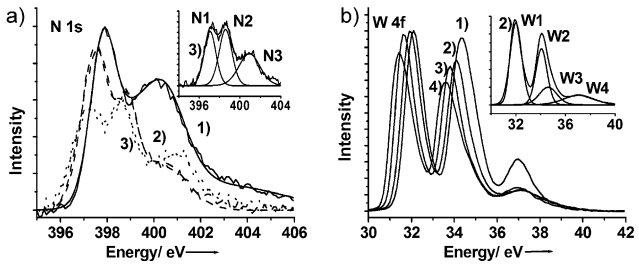

Figure 3. XPS a) N 1s spectra of 1) CN, 2) WCN and 3) Fe-WCN materials prepared at 800 °C; the inset shows the deconvoluted XPS N 1s spectra of Fe-WCN-800 (3). b) W 4f spectra of Fe-WCN catalysts prepared at various temperatures. 1) Fe-WCN-700, 2) Fe-WCN-800, 3) Fe-WCN-900, and 4) Fe-WCN-1000. The inset shows the deconvoluted XPS W 4f spectra of Fe-WCN-800 (2). W1 and W2 are N-bound W atoms, W3 and W4 are O-bound W atoms.

400.4 eV), according to their binding energies (Figure 3a, inset).[8] The peak at 400.4 eV was assigned to a quaternary N atom. Compared to CN, a new N 1s peak appeared at 398.8 eV in the WCN and Fe-WCN materials, and was assigned to a W-bound N species. The binding energy of the original pyridinic N in the CN materials was 397.8 eV, but shifted to a higher binding energy (398.8 eV), implying that electrons in the N atoms are donated to the W species.[9]

To better understand the nature of the active catalytic sites, we attempted to control the amount of N-bound W species in the synthesized Fe-WCN materials. During the pyrolysis process, it is well documented that nitrogen atoms escape from the substrates.[10] Thus, we anticipated that Fe-WCN materials with different concentrations of nitrogen could be synthesized by adjusting the pyrolysis temperatures. To this end, we pyrolyzed the Fe-WCN materials at 700 °C, 800 °C, 900 °C, and 1000 °C, and defined the resulting catalysts as Fe-WCN-700, Fe-WCN-800, Fe-WCN-900, and Fe-WCN-1000, respectively. The surface elemental state of the Fe-WCN catalysts was examined also by XPS (Figure 3b; see also Figure S5 and Table S2). As expected, increasing the pyrolysis temperatures resulted in a lower content of N species. The pyrolysis temperature also affects the electronic state of the W species. As shown in Figure 3b, the W 4f XPS spectra of the Fe-WCN catalysts were deconvoluted into four peaks, which were assigned to two types of W species, a N/C-bound (W1 and W2) type and an O-bound (W3 and W4) type, based on their respective binding energies.[11] The XPS peaks of Fe-WCN-800 at 32.2 eV (W1) and 34.1 eV (W2) were assigned to N-bound W atoms, which is the dominant W species (74.1 %). Notably, this peak exhibited a lower-energy shift with increasing pyrolysis temperature due to the loss of N atom content in the Fe-WCN materials. This finding demonstrates that the W-bound N species substantially decreased the electron density of the W atoms, resulting in a downshift of the d band of W active sites. The N atom content (6.1 at %) in Fe-WCN-800 was markedly higher than that of Fe-WCN-1000 (3.8 at %), demonstrating that the N atom concentration of the Fe-WCN materials gradually decreased with increasing pyrolysis temperature (between 800–1000 °C).

The loss of N atom content in the Fe-WCN materials with increasing pyrolysis temperature was further confirmed by XRD analysis (Figure S6). WN species in Fe-WCN-800 exhibited well-defined XRD peaks at 31.6°, 35.7°, 48.4°, 64.2°, 73.3°, 75.7°, and 77.3°, corresponding to the 001, 100, 101, 110, 002, 111, 200, and 102 planes of WN, respectively (JCPDS PDF 65-9410). No impurity peaks from WO_3 or W were observed. As shown in the enlarged XRD spectra, the peaks at 64.2°, 73.3°, 75.7°, and 77.3° were negatively shifted after increasing the pyrolysis temperature, which was due to the formation of W–C bonds (JCPDS PDF 65-4539).

The HER activities of Fe-WCN materials synthesized at different temperatures were evaluated by measuring polarization curves (Figure S7). Increasing the pyrolysis temperature to 800–1000 °C resulted in a negative shift of the overpotential, with the Fe-WCN-800 catalyst displaying the highest HER activity. Tafel curves in the low-current-density regions of Figure 2 were plotted with that of Pt/C as a reference (Figure S8). The Tafel slope of Fe-WCN-800 catalyst was calculated to be 47.1 mV dec^{-1}, which is the highest HER kinetic activity among the Fe-WCN catalysts (Table 1). We also evaluated the current density based on the electrochemical active surface area (EASA; Table 1; see also Figures S9 and S10), and found that Fe-WCN-800 also had the highest HER current density (0.110 mA cm^{-2}). The HER kinetic activity of Fe-WCN-800 was slightly lower than that of Pt/C (31 mV dec^{-1}). Although Fe-WCN-700 was found to have a higher content of nitrogen species than that of Fe-WCN-800 (Table S2), Fe-WCN-700 displayed a lower HER activity. This property is likely due to the lower electrical resistivity and specific surface area of Fe-WCN-700 (20 Ω cm and 100 $m^2 g^{-1}$; see the Supporting Information for the method) compared to that of Fe-WCN-800 (0.5 Ω cm, 127.2 $m^2 g^{-1}$; Table 1 and Figure S9). In the Fe-WCN-800 and Fe-WCN-900 samples, the W and Fe contents estimated from the XPS analysis were almost the same; however, Fe-WCN-800 had a higher N atom content. Together, these findings demonstrate that N-bound W species are related to the HER activity of Fe-WCN materials. One more experiment through electrochemical oxidation of Fe-WCN materi-

Table 1: Characterization and activity data for Fe-WCN catalysts synthesized at different temperatures.

T_{syn} [°C]	W-bound N[a] [atom %]	Conductivity [Ω cm]	BET surface area [$m^2 g^{-1}$]	EASA [$m^2 g^{-1}$]	Tafel slope [mV dec^{-1}]	J[b] GSA [mA cm^{-2}]	J[b] EASA [mA cm^{-2}]
700	2.5	20	100.2	9.8	52.4	2.9	0.074
800	2.2	0.5	127.2	12.5	47.1	5.5	0.110
900	1.6	0.4	177.9	16.4	51.6	3.6	0.055
1000	0.5	0.2	196.0	17.8	53.7	2.6	0.036

[a] 398.8 eV. [b] at −0.2 V. EASA = electrochemically active surface area, GSA = geometric surface area (0.2 cm^2), J = current density, T_{syn} = temperature of synthesis.

als in situ further proved that N-bound W species are the HER active sites. Details can be found in Table S3 and Figures S11 and S12.

The HER activity of electrocatalysts is strongly related to metal-hydrogen bonding, for which the optimized strength can be estimated from volcano plots.[12] Tafel slopes of the Fe-WCN catalysts (Figure S8) indicated that the HER possibly occurred through a Volmer–Heyrovsky mechanism,[4,13] in which a proton reacts with H_{ads} and a second electron on the catalyst surface to generate H_2 as the limiting step.[14] We propose that the high HER activity of the synthesized Fe-WCN catalysts was due to the existence of N-bound W species. The W atoms in WN are more positively charged than those in WC due to the higher electronegativity of N (3.04) compared to C (2.55), as evidenced by the XPS analysis. This coordination structure substantially downshifted the d-band center of the W atoms, resulting in the weakened W−H bonding that facilitated desorption of H_{ads} atoms from the catalyst surface.[4]

Finally, we compared the HER activity of the Fe-WCN material to one prepared by the conventional method (c-Fe-WCN), that is, direct ammonification of $WO_3/Fe(NO_3)_3$/carbon hybrids. As shown in Figure 2b (circle curve), the generated HER currents and onset-potentials ($-0.25\ V_{RHE}$) of c-Fe-WCN are substantially lower than our new Fe-WCN materials. Figure S13 compares the W 4f and N 1s XPS spectra of c-Fe-WCN and Fe-WCN materials, and Table S4 summarizes their surface elemental contents. A large amount of WO_3 species was detected (36.9 eV and 34.9 eV) in c-Fe-WCN samples, which indicates that the c-Fe-WCN material suffered incomplete ammonification. The W atom contents are similar (ca. 10 atom%), whereas the N atom content (1.2 atom%) in c-Fe-WCN is much lower than in our Fe-WCN materials (6.1 atom%). Thus, low N-content and poor ammonification of c-Fe-WCN materials leads to the low HER activity observed, which reveals that our novel synthetic method is an effective way to fabricate N-rich tungsten nitride (WN) with very high activity.

In summary, we have described a new synthetic route for preparing N-rich Fe-WCN core-shell nanomaterials with small-sized particles and crystalline structure, which function as efficient HER electrocatalysts. The homogeneous release of protons from the polymerization process provides a unique synthetic route to H_2WO_4 nanoparticles, which were then used to synthesize WN-derived materials. We believe that even more efficient catalysts can be fabricated by further increasing both the density of N-bound W species and the specific surface area. Equally important, this strategy is also anticipated to be suitable for synthesizing other functional metallic nitrides, such as molybdenum nitride, niobium nitride, and tantalum nitride,[15] which are advanced catalytic materials used in various systems, such as lithium ion batteries and fuel cells.

Received: August 27, 2013
Published online: October 23, 2013

Keywords: electrocatalysts · hydrogen evolution · nanostructures · tungsten carbonitride

[1] a) W. Q. Zheng, T. P. Cotter, P. Kaghazchi, T. Jacob, B. Frank, K. Schlichte, W. Zhang, D. S. Su, F. Schuth, R. Schlogl, *J. Am. Chem. Soc.* **2013**, *135*, 3458–3464; b) M. X. Wu, X. A. Lin, A. Hagfeldt, T. L. Ma, *Angew. Chem.* **2011**, *123*, 3582–3586; *Angew. Chem. Int. Ed.* **2011**, *50*, 3520–3524; c) D. V. Esposito, S. T. Hunt, Y. C. Kimmel, J. G. G. Chen, *J. Am. Chem. Soc.* **2012**, *134*, 3025–3033; d) B. Keita, U. Kortz, L. R. B. Holzle, S. Brown, L. Nadjo, *Langmuir* **2007**, *23*, 9531–9534; e) B. Keita, S. Floquet, J. F. Lemonnier, E. Cadot, A. Kachmar, M. Benard, M. M. Rohmer, L. Nadjo, *J. Phys. Chem. C* **2008**, *112*, 1109–1114.

[2] R. B. Levy, M. Boudart, *Science* **1973**, *181*, 547–549.

[3] a) M. L. Frauwallner, F. Lopez-Linares, J. Lara-Romero, C. E. Scott, V. Ali, E. Hernandez, P. Pereira-Almao, *Appl. Catal. A* **2011**, *394*, 62–70; b) N. Ji, T. Zhang, M. Y. Zheng, A. Q. Wang, H. Wang, X. D. Wang, J. G. G. Chen, *Angew. Chem.* **2008**, *120*, 8638–8641; *Angew. Chem. Int. Ed.* **2008**, *47*, 8510–8513; c) F. H. Ribeiro, R. A. D. Betta, G. J. Guskey, M. Boudart, *Chem. Mater.* **1991**, *3*, 805–812; d) W. T. Yu, Z. J. Mellinger, M. A. Barteau, J. G. G. Chen, *J. Phys. Chem. C* **2012**, *116*, 5720–5729.

[4] W. F. Chen, K. Sasaki, C. Ma, A. I. Frenkel, N. Marinkovic, J. T. Muckerman, Y. M. Zhu, R. R. Adzic, *Angew. Chem.* **2012**, *124*, 6235–6239; *Angew. Chem. Int. Ed.* **2012**, *51*, 6131–6135.

[5] a) S. M. Wang, X. H. Yu, Z. J. Lin, R. F. Zhang, D. W. He, J. Q. Qin, J. L. Zhu, J. Han, L. Wang, H. K. Mao, J. Z. Zhang, Y. S. Zhao, *Chem. Mater.* **2012**, *24*, 3023–3028; b) H. M. Wang, W. Li, M. H. Zhang, *Chem. Mater.* **2005**, *17*, 3262–3267; c) H. Vrubel, X. L. Hu, *Angew. Chem.* **2012**, *124*, 12875–12878; *Angew. Chem. Int. Ed.* **2012**, *51*, 12703–12706.

[6] S. Izhar, H. Kanesugi, H. Tominaga, M. Nagai, *Appl. Catal. A* **2007**, *317*, 82–90.

[7] C. K. Gu, B. C. Norris, F. R. F. Fan, C. W. Bielawski, A. J. Bard, *ACS Catal.* **2012**, *2*, 746–750.

[8] Y. Zhao, K. Watanabe, K. Hashimoto, *J. Am. Chem. Soc.* **2012**, *134*, 19528–19531.

[9] a) K. Artyushkova, S. Levendosky, P. Atanassov, J. Fulghum, *Top. Catal.* **2007**, *46*, 263–275; b) K. Kamiya, K. Hashimoto, S. Nakanishi, *Chem. Commun.* **2012**, *48*, 10213–10215.

[10] Y. Zhao, R. Nakamura, K. Kamiya, S. Nakanishi, K. Hashimoto, *Nat. Commun.* **2013**, *4*, 2390.

[11] C. Shi, X. F. Yang, A. M. Zhu, C. T. Au, *Catal. Today* **2004**, *93–5*, 819–826.

[12] a) M. M. Jaksic, *Int. J. Hydrogen Energy* **2001**, *26*, 559–578; b) M. T. M. Koper, *Nat. Chem.* **2013**, *5*, 255–256.

[13] a) E. Navarro-Flores, Z. W. Chong, S. Omanovic, *J. Mol. Catal. A* **2005**, *226*, 179–197; b) N. Danilovic, R. Subbaraman, D. Strmcnik, K. C. Chang, A. P. Paulikas, V. R. Stamenkovic, N. M. Markovic, *Angew. Chem.* **2012**, *124*, 12663–12666; *Angew. Chem. Int. Ed.* **2012**, *51*, 12495–12498.

[14] E. Skúlason, V. Tripkovic, M. E. Björketun, S. Gudmundsdóttir, G. Karlberg, J. Rossmeisl, T. Bligaard, H. Jónsson, J. K. Nørskov, *J. Phys. Chem. C* **2010**, *114*, 22374–22374.

[15] a) R. Ohnishi, K. Takanabe, M. Katayama, J. Kubota, K. Domen, *J. Phys. Chem. C* **2013**, *117*, 496–502; b) M. H. Yang, F. J. DiSalvo, *Chem. Mater.* **2012**, *24*, 4406–4409.

